Korean J. Chem. Eng., 34(4), 1004-1012 (2017)
DOI: 10.1007/s11814-017-0016-2

pISSN: 0256-1115
eISSN: 1975-7220

Effect of sulfidation process on catalytic performance over unsupported Ni-Mo-W hydrotreating catalysts

Changlong Yin† and Yiyan Wang

State Key Laboratory of Heavy Oil Processing and Key Laboratory of Catalysis of CNPC, China University of Petroleum (East China), Qingdao 266580, P. R. China
(*Received 19 September 2016 • accepted 2 February 2017*)

Abstract−Oxidic unsupported Ni-Mo-W catalysts were chosen to elucidate the effect of sulfidation conditions on the catalytic performance. The catalysts were sulfided in situ by using dimethyl sulfide as sulfiding agent. The relationships between the time needed for sulfidation and the sulfiding conditions were studied by GC-analysis method. Straight-run gas oil with high sulfur and nitrogen content was used to evaluate the hydrotreating performance. The oxidic catalyst precursors and sulfided catalysts were characterized by X-ray diffraction (XRD), high-resolution transmission electron microscopy (HRTEM), and X-ray photoelectron spectroscopy (XPS). With increasing sulfiding liquid hourly space velocity (LHSV) of the sulfiding agent, the reaction time necessary for the sulfidation decreased, while the activity of the catalyst increased significantly. The higher catalytic activity might be due to the MoS_2/WS_2 slabs with shorter length and higher stacking number, which might contribute to the catalyst with more active sites. Sulfiding at 330 °C took the longest sulfidation time, while the catalytic activity was also the highest after sulfiding at this temperature. Furthermore, within a certain range, the sulfidation pressure had no evident effect on the catalytic behavior or activity. The purpose of this work was to provide a basis for actual production and a reference for further research.

Keywords: Sulfidation, Unsupported Hydrotreating Catalysts, Hydrodesulfurization, NiMoW Catalyst, Gas Oil

INTRODUCTION

The increasing demand for high quality diesel fuel has put pressure on the development of the hydroprocessing process, and intensive attention has been paid to transition metal catalysts with higher activity [1,2]. Hydrotreating catalysts are generally comprised of molybdenum or tungsten with nickel or cobalt as promoter and alumina as support [3]. As a representative unsupported catalyst, NEBULA is a Ni-Mo-W trimetallic catalyst with a three-times higher activity than supported hydrotreating catalysts [4]. Due to their higher concentration of active sites, unsupported catalysts have higher activities for hydrodesulfurization (HDS), hydrodenitrogenation (HDN), and aromatics saturation than supported catalysts [5,6]. Unsupported catalysts have been prepared by different methods, including chemical precipitation, hydrothermal reaction, and thiosalt decomposition [7-9], and generally described as oxide catalysts [10,11] and sulfide catalysts [12,13] depending on their composition.

Sulfidation is crucial for obtaining highly active catalysts, and diverse sulfiding agents have been used, such as sulfur powder, hydrogen sulfide (H_2S), carbon disulfide (CS_2), dimethyl sulfide (DMS), dimethyl disulfide (DMDS), and ditertiary nonyl polysulfide (TNPS) [14-16]. Gochi et al. [4] studied the effect of H_2S, DMS, and DMDS on Mo-W-Ni unsupported catalysts, and the result showed that the catalyst sulfided by DMS had the highest surface area, favoring the direct desulfurization pathway (DDS). Füchtbauer et al. [16] investigated the atomic-scale structure of MoS_2 nanoclusters sulfided with H_2S, DMS, and DMDS and found that sulfiding with the less strongly sulfiding agent DMS could partially imitate industrial conditions by giving rise to a lower sulfur coverage (50%) on the Mo-edge, which is supposed to be the most stable Mo-edge under hydrotreating conditions [17,18]. Berhault et al. [19] found that more highly dispersed MoS_2 crystallites had formed in an unsupported catalyst after DMS treatment. The active phase of a hydrotreating catalyst is also affected by the sulfiding conditions [20-22], and many investigations have been carried out. Amaya et al. [23,24] found that the sulfiding temperature had a large effect on the structural, textural, and morphological properties of a sulfided Ni-Mo-W catalyst. With increasing activation temperature, the crystallinity of the material increased, while the surface area and pore volume decreased, and the catalyst presented a higher tendency to agglomerate. At the same time, the influence of the sulfidation pressure on the structure and activity of the HDS catalyst was studied by Dugulan et al. [25], and the results suggested that the catalyst sulfided at higher pressure had a considerably higher HDS activity. The fully sulfided Co species at higher pressure and the easier formation of Type II Co-Mo-S phase, which was twice as active as Type I [26], may explain this improvement.

Because crucial changes of the catalytic performance may occur as a function of the sulfiding conditions, it is important to study the sulfidation process relevant to industrial practice. However, seldom work has been reported about the sulfidation behavior of unsupported catalysts with real feeds, which has significant reference value for actual production. In this work, an unsupported Ni-Mo-

†To whom correspondence should be addressed.
E-mail: catgroup@upc.edu.cn

W catalyst was activated with DMS as sulfiding agent. The effect of the sulfiding conditions (LHSV, temperature, and pressure) on the sulfidation behavior was studied by the measurement of the sulfur content in the exhaust gas. The sulfidation was carried out with sampling being performed every hour and analysis with gas chromatography. The sulfided catalysts were evaluated with the straight-run gas oil (SRGO) with high sulfur and nitrogen content produced by West Pacific Petrochemical Company Ltd. Dalian (WEPEC).

EXPERIMENTAL

1. Synthesis of Ammonium Nickel Molybdates

The reagents used were purchased from Sinopharm Chemical Reagent Company (PR China, Grade AR). Basic nickel carbonate ($NiCO_3 \cdot 2Ni(OH)_2 \cdot 4H_2O$), ammonium heptamolybdate ($(NH_4)_6Mo_7O_{24} \cdot 4H_2O$), and ammonium metatungstate ($(NH_4)_6W_7O_{24} \cdot 6H_2O$) were mixed in the molar ratio Ni : Mo : W=2 : 1 : 1 with some deionized water. The liquid mixture was transferred to an autoclave and reacted at 150 °C for 10 h. After cooling to room temperature, the product was isolated by vacuum filtration, dried overnight at 120 °C, and the Ni-Mo-W precursor was obtained.

2. Preparation of Unsupported Catalyst

The precursor was mixed with alumina gel binder (65/35 by weight) and extruded into rods 1.6 mm in diameter. The extrudates were dried at 120 °C for 12 h and calcined at 300 °C for 4 h, and then crushed into 20-40 mesh particles. Oxidic unsupported Ni-Mo-W catalyst was obtained.

3. Sulfidation and Activity Evaluation of Unsupported Catalyst

The in situ sulfidation of the unsupported catalyst was done in a 20 ml fixed-bed down-flow micro-reactor, with a 3 wt% DMS-kerosene solution as the sulfiding agent. The sulfiding reaction was carried out at a H_2/feed ratio of 600. The LHSV of the sulfiding agent, sulfiding temperature, and sulfiding pressure were varied. The exhaust gas was analyzed using a Varian 3800 gas chromatograph equipped with a pulse flame photometric detector (PFPD).

After sulfidation, SRGO was used as evaluation feed; the characteristics of the SRGO are presented in Table 1. The sulfur and nitrogen content of the gas oil were determined with a MultiEA3100 (Analytikjena) trace element analyzer. The reaction conditions were: temperature 340 °C, pressure 6.0 MPa, H_2/feed ratio 600, and LHSV 2.0 h^{-1}. Liquid products were analyzed by using a 450-GC gas chromatograph (Bruker) equipped with a flame ionization detector (FID) and 30 m HP-5 capillary column.

4. Characterization of Sulfide Catalysts

The sulfided samples were transferred into a glove box without air exposure. The XRD characterization of the crystal structure of the sulfided catalysts was performed with an X'Pert Pro MPD diffraction instrument (Panalytical) with a scintillation counter detector, from 5° to 75° at a rate of 5°/min, and the sulfided samples were treated with an argon flow to avoid the oxidation. HRTEM experiments were performed on a JEM 2100 microscope operated at 200 kV with a LaB6 filament. To compare the sulfided catalysts in detail, statistical analysis was carried out. The average slab length (L_A) and average number of layers (N_A) were calculated according to Eqs. (1) and (2), where L_i is the length of slab i, N_i is the number of layers in slab i, and n_i is the number of slabs.

$$L_A = \sum_{i=1}^{t} n_i L_i / \sum_{i=1}^{t} n_i \quad (1)$$

$$N_A = \sum_{i=1}^{t} n_i N_i / \sum_{i=1}^{t} n_i \quad (2)$$

The samples were ground and pressed into an indium foil and transported into the preparation chamber of the XPS machine. XPS analysis was on an Axis ultra DLD spectrometer (Kratos Analytic) by using monochromatic Al Kα radiation (1486.6 eV) with a spot size of 500 mm and an excitation power of 300 V. The elemental surface composition of the sulfided Ni-Mo-W catalysts was determined from the intensity of the metal (Ni 2p, Mo 3d, and W 4f) and sulfur (S 2p) peaks provided by the manufacturer of the XPS apparatus. Binding energies (BEs) were determined with C 1s (284.6 eV) as reference.

Table 1. Main characteristics of the SRGO

Properties	SRGO
Sulfur concentration (μg/g)	13940
Total nitrogen concentration (μg/g)	161
Density at 20 °C (g/mL)	0.8485
Initial boiling point (°C)	202
Final boiling point (°C)	365

RESULTS AND DISCUSSION

1. Effect of Sulfiding Agent LHSV

1-1. Sulfidation Process

In the presence of hydrogen, DMS produces hydrogen sulfide in accordance with Eq. (3). Based on previous study [27], DMS did not undergo hydrogenolysis below 230 °C. Reactions (4-6) were supposed to occur on the oxide Ni-Mo-W catalyst.

$$CH_3SCH_3 + 2H_2 \rightarrow H_2S + 2CH_4 \quad (3)$$

$$MoO_3 + H_2 + 2H_2S \rightarrow MoS_2 + 3H_2O \quad (4)$$

$$3NiO + H_2 + 2H_2S \rightarrow Ni_3S_2 + 3H_2O \quad (5)$$

$$WO_3 + H_2 + 2H_2S \rightarrow WS_2 + 3H_2O \quad (6)$$

The curves of the sulfiding temperature and the content (volume percentage) of the main sulfur compounds in the exhaust changed with the sulfiding time at different LHSV, and the results are in Fig. 1 (The flow rate of DMS were 0.19, 0.38, and 0.57 mmol S/h g-cat correspond to 1, 2, and 3 h^{-1} LHSV of sulfiding agent, respectively). The sulfiding temperature was increased from room temperature to 330 °C at a rate of 40 °C/h after the introduction of the sulfiding agent. The specific process of the sulfidation can be obtained based on the fluctuation of the content of the sulfur compounds in the exhaust gas. Taking Fig. 1(a) as an illustration, the whole sulfidation process can be divided into four stages: (1) Physical absorption of DMS (0-3 h); (2) Once the adsorption is complete, DMS is detected (3-5 h); (3) The decomposition of DMS shows that sulfidation began (5-18 h); and (4) The abrupt increase

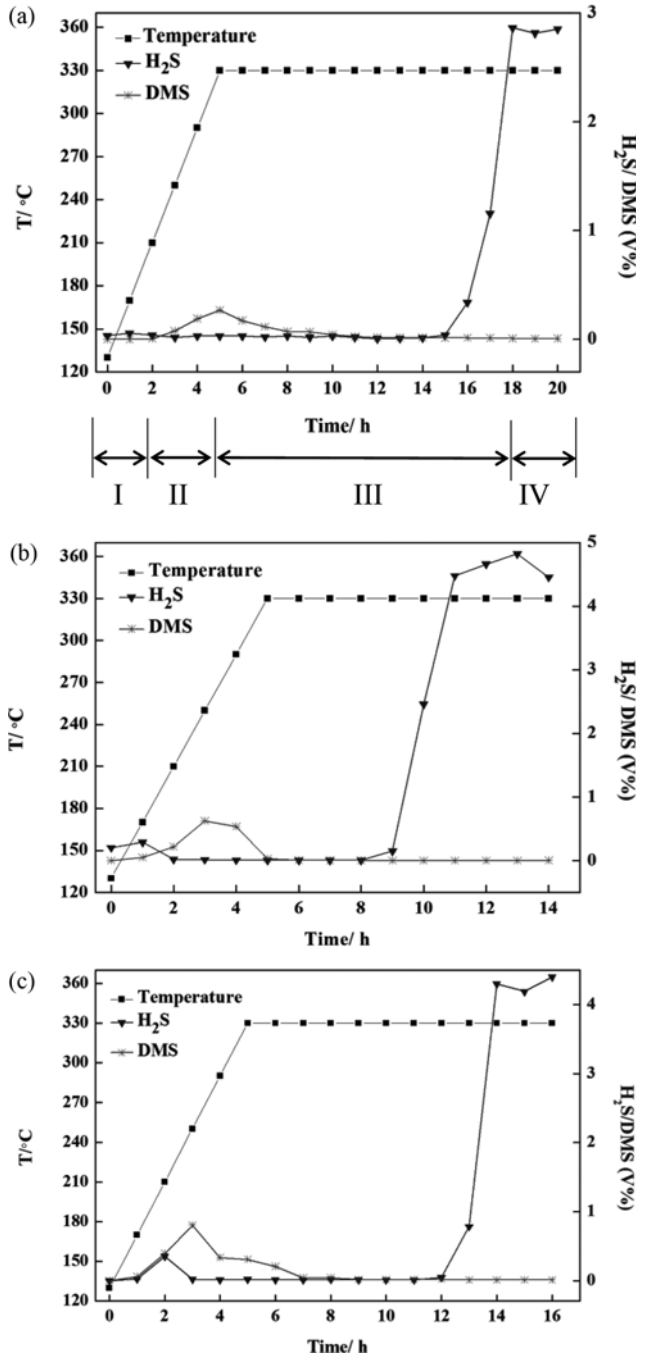

Fig. 1. Curves of temperature and content of main sulfides in exhaust changing with time with different sulfiding LHSV ((a) 1 h^{-1}, (b) 2 h^{-1}, (c) 3 h^{-1}).

of H_2S demonstrates the completion of sulfidation (after 18 h).

The content of DMS remained zero because of the physical adsorption at stage one, and then increased slightly due to the saturation at stage two. After that, DMS started to decompose into H_2S and CH_4 with further increasing temperature at the initial third stage and was basically undetectable during the final stages. All the H_2S resulted from the decomposition of the DMS involved in the sulfidation. Therefore, the content of H_2S in the exhaust gas remained at a near-zero level before the third stage and then increased dramatically to a stable level at the end of the sulfidation process. From this it can be concluded that the sulfidation finished after the third stage. Therefore, the reaction time of the sulfidation (the whole time of the third stage) at LHSV of 1, 2, and 3 h^{-1} was 13, 11, and 8 h, respectively. The results show that with increasing sulfiding LHSV, the reaction time necessary for the sulfidation decreased. This might be understood in terms of more sufficient sulfiding agent involved in the whole process of sulfidation when sulfiding at higher LHSV.

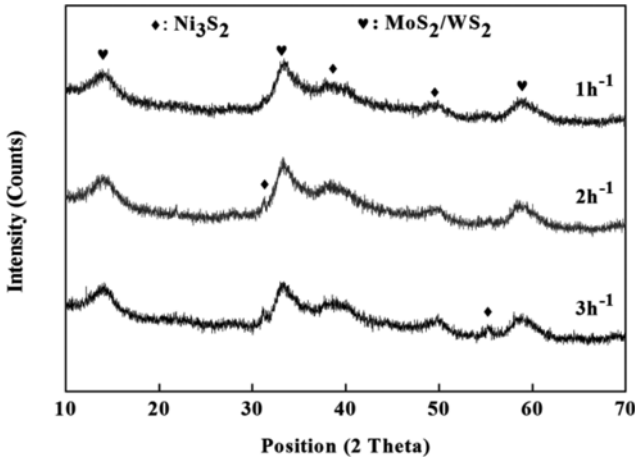

Fig. 2. XRD patterns of sulfided Ni-Mo-W catalysts with different sulfiding LHSV.

1-2. XRD

The sulfided unsupported Ni-Mo-W catalysts prepared at different LHSV were characterized by XRD (Fig. 2), and it could be found that all the samples had similar characteristics of the diffraction peaks of Ni_3S_2 and MoS_2/WS_2 nanoparticles. The typical peak due to the stacking of the MoS_2/WS_2 slabs along the c-axis was present at 2θ 14.4° (0 0 2) [28,29]. This typical (0 0 2) peak of MoS_2/WS_2 has been related to the catalytic activity of the catalysts [30, 31]. The XRD peaks of Ni_3S_2 (JCPDS card No. 44-1418) were hardly observed, especially at lower LHSV, implying that nickel sulfide species were either composed of small crystallites or completely amorphous. With increasing sulfiding LHSV, the intensity of the MoS_2/WS_2 peaks remained basically unchanged, while the intensity of the Ni_3S_2 peaks increased slightly, indicating that the sulfiding LHSV had little effect on the distribution and particle size of Ni_3S_2 and MoS_2/WS_2 species. Altamirano et al. [32] proposed that the coincident formation of Ni_3S_2 and MoS_2 might be due to the decomposition of the 'NiMoS' active phase ($NiMoS \rightarrow Ni_3S_2+MoS_2$). In that case, the simultaneous detection of Ni_3S_2 and MoS_2 for the Ni-Mo-W catalyst might be beneficial for the HDS reaction. It was also reported that a good dispersion of the Ni promoter on MoS_2 is necessary for the formation of a large number of 'NiMoS' active phase [33]. However, the 'NiMoS' phase was possibly present in the form of small nano-sized particles, which cannot be detected by XRD [34].

1-3. Catalytic Activity

SRGO was used as a model to evaluate the activity of the catalysts. Table 2 and Fig. 3 present the activity data of the catalysts after sulfiding at different LHSV. The sulfur and nitrogen content and

Table 2. Influence of sulfiding LHSV on catalytic activities

LHSV/h^{-1}	ρ/(g/ml)	S/(μg/g)	N/(μg/g)
Gas oil	0.8485	13940	161
1.0	0.8248	119.3	1.2
2.0	0.8243	63.4	0.8
3.0	0.8243	63.2	0.8

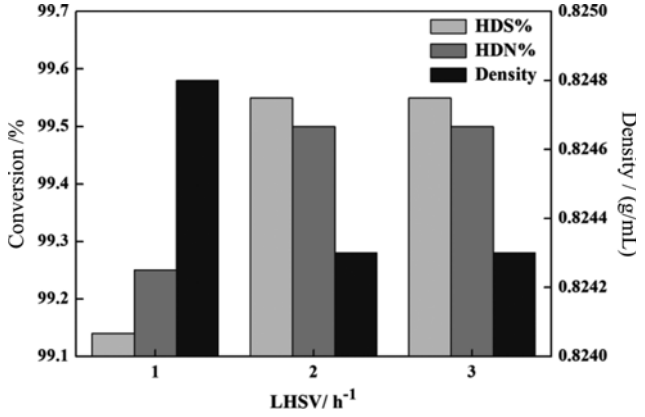

Fig. 3. Influence of sulfiding LHSV on activity of the unsupported Ni-Mo-W catalysts.

the density of the gas oil decreased dramatically after catalytic hydrogenation (Table 2), while the desulfurization and denitrogenation degree of all the catalysts reached over 99% (Fig. 3). The activity of the catalyst after sulfiding at 2 or 3 h^{-1} was higher than at 1 h^{-1}. The higher LHSV contributed to the higher activity of the catalyst, which might be due to the different morphology of the MoS_2/WS_2 slabs, as confirmed by HRTEM analysis.

According to the results of the sulfiding LHSV and reaction time, the demand of the sulfiding agent for the sulfidation at 3 h^{-1} was the highest. Within a certain range, it is reasonable to sulfide with a higher LHSV of sulfiding agent to improve the catalytic activity and reduce the time needed for the sulfidation. However, a higher sulfiding LHSV may cause excessive consumption of sulfiding agent. Since the effects of sulfidation at 2 h^{-1} and 3 h^{-1} were basically the same, taking the practical production into consideration, excessively high sulfiding LHSV is disadvantageous, which could lead to the higher cost of production and equipment load. Therefore, in the following sections, we will only compare the sulfidation at 2 and 1 h^{-1}.

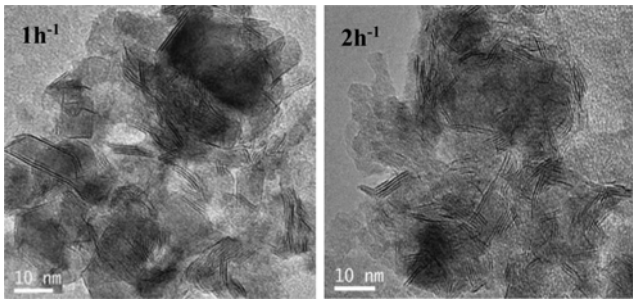

Fig. 4. HRTEM images of sulfided Ni-Mo-W catalysts with different sulfiding LHSV.

1-4. HRTEM Characterization

Fig. 4 shows the HRTEM images of the unsupported Ni-Mo-W catalyst after sulfiding LHSV 1 and 2 h^{-1}. The black streak lines are the MoS_2/WS_2 crystal slabs. The statistical analysis of the length and the stacking layer number distributions of the MoS_2/WS_2 slabs of the sulfided Ni-Mo-W catalysts with different sulfiding LHSV are presented in Fig. 5.

The representative black MoS_2/WS_2 layers (interplanar distance of the typical (002) basal planes is around 0.62 nm) were observed in all the catalysts [10,35]. The MoS_2/WS_2 average slab length and stacking number were calculated. When the sulfiding LHSV was 1 h^{-1}, almost 60% of the observed MoS_2/WS_2 slabs was between 5 and 7 nm long (Fig. 5), and the average length is 6.9 nm, which is longer than 5.5 nm on the catalyst sulfided at 2 h^{-1}. Fig. 5 shows that over 80% of the observed MoS_2/WS_2 slabs having three to five layers on the catalyst sulfided at 2 h^{-1}, and the average stacking number was 4.3, which is higher than 3.8 on the catalyst sulfided at 1 h^{-1}. It is widely acknowledged that the hydrodesulfurization activity of the catalyst is higher when the MoS_2/WS_2 slabs have shorter length and higher stacking number [30]. No significant Ni_3S_2 lamellas (interplanar spacing of about 0.29 nm) were found, indicating that the Ni_3S_2 phase might be well dispersed in all the catalysts. According to the HRTEM result, sulfiding at 2 h^{-1} is beneficial, giving

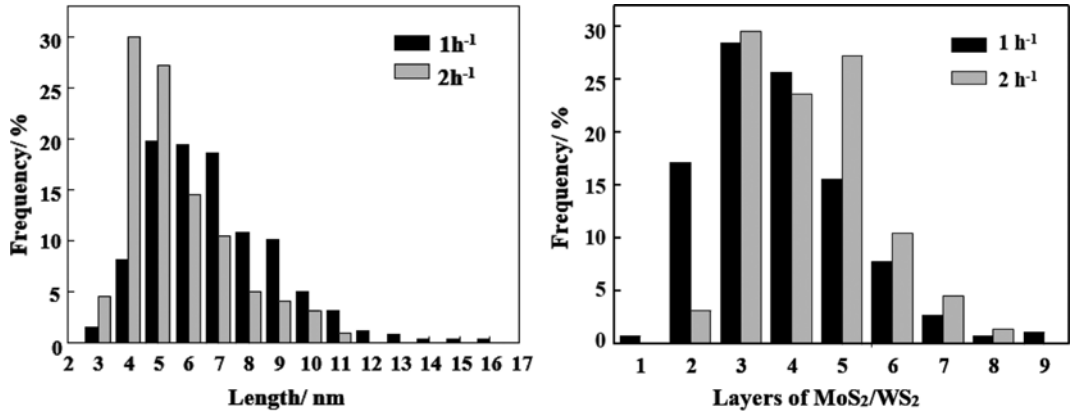

Fig. 5. The slab length and stacking number of MoS_2/WS_2 with different sulfiding LHSV.

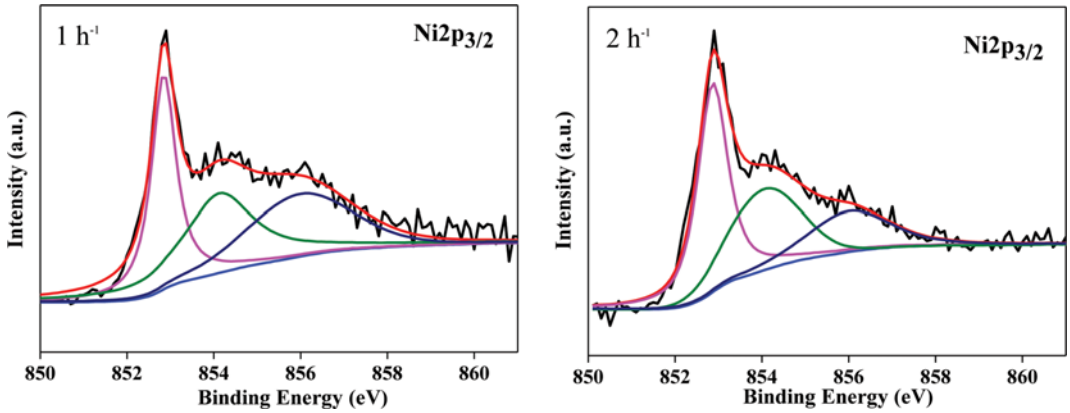

Fig. 6. Ni2p XPS spectra of the sulfided catalysts with different sulfiding LHSV.

MoS_2/WS_2 slabs with shorter length and higher stacking number, which contributes to a higher catalytic activity.

1-5. XPS

The XPS spectra of the sulfided catalysts were collected and decomposed using an iterative least-squares computer program, XPSPEAK version 4.1 [36]. The Ni 2p, Mo 3d, and W 4f XPS spectra of the catalysts are shown in Figs. 6-8, and the corresponding parameters are reported in Table 3.

The Ni $2p_{3/2}$ XPS spectra of the sulfided catalysts are shown in Fig. 6. XPS peaks located at 853.0±0.2 and 853.8 eV±0.2 eV were attributed to NiS_x (i.e., Ni_9S_8, Ni_3S_2, or NiS) and Ni (II) embedded in the structure of WS_2 or MoS_2, probably forming the Ni-Mo (W)-S phase [37], respectively. Besides, an XPS peak centered at 856.0±0.2 eV was indicated of Ni (II) oxide compounds [38]. The fraction of sulfided nickel of the catalyst sulfided at 2 h^{-1} was 79%, which is significantly higher than that of the catalyst sulfided at 1 h^{-1} (69%) (Table 3). This implies that sulfiding the catalyst at 2 h^{-1} enhances the sulfidation of Ni species, which agrees with the XRD result (Fig. 2).

Table 3. XPS parameters of Ni 2p, Mo 3d and W 4f of the sulfided catalysts sulfided with different sulfiding LHSV

LHSV/ h^{-1}	Binding energy/(eV)					
	Ni sulfide		Ni oxide	Mo^{IV}	W^{IV}	W^{VI}
1.0	852.8 (31.9)[a]	854.1 (37.7)	856.1 (30.4)	229.0 (100)	32.2 (68.4)	34.4 (31.6)
2.0	852.9 (46.3)	854.0 (32.8)	856.0 (20.9)	229.0 (100)	32.1 (76.4)	34.3 (23.6)

[a]Values in parentheses are the percentages of the area of the deconvoluted peak with respect to the total area of the peak

The Mo 3d XPS spectra of the sulfided catalysts are shown in Fig. 7. Molybdenum exist as disulfide (MoS_2) is located at 228.8± 0.2 eV (Mo^{IV} $3d_{5/2}$) and 232.0±0.2 eV (Mo^{IV} 3d3/2) [39]. And a broad peak at 226.0±0.2 eV was ascribed to sulfur (S 2s) line and subtracted from the total spectra of Mo 3d [16]. No peak due to Mo oxide species was observed [39], indicating full sulfidation of Mo species of both catalysts.

The W 4f XPS spectra of the sulfided catalysts are shown in Fig. 8. The more intense XPS peaks located at 32.0±0.2 eV (W $4f_{7/2}$) and 34.2±0.2 eV (W $4f_{5/2}$) are ascribed to W^{IV} species in a WS_2-like structure, indicating that during the sulfidation process reduction of W^{VI} to W^{IV} took place. XPS peaks at 35.5±0.2 eV (W $4f_{7/2}$) and 37.7±0.2 eV (W $4f_{5/2}$) are assigned to unreduced W^{VI} in an oxygen environment [40], although it is not possible to establish if this signal corresponds to WO_3 or $NiWO_4$, since both substances show very similar binding energy values [41,42]. Table 3 presents the per-

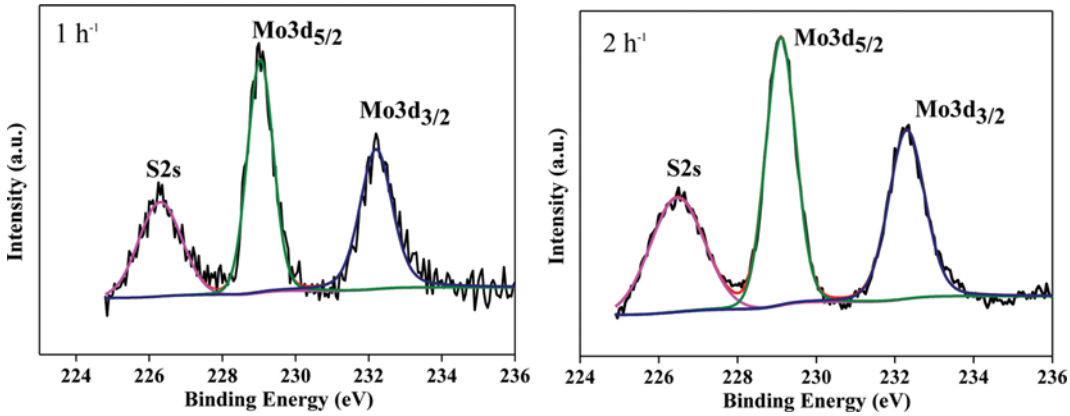

Fig. 7. Mo3d XPS spectra of the sulfided catalysts with different sulfiding LHSV.

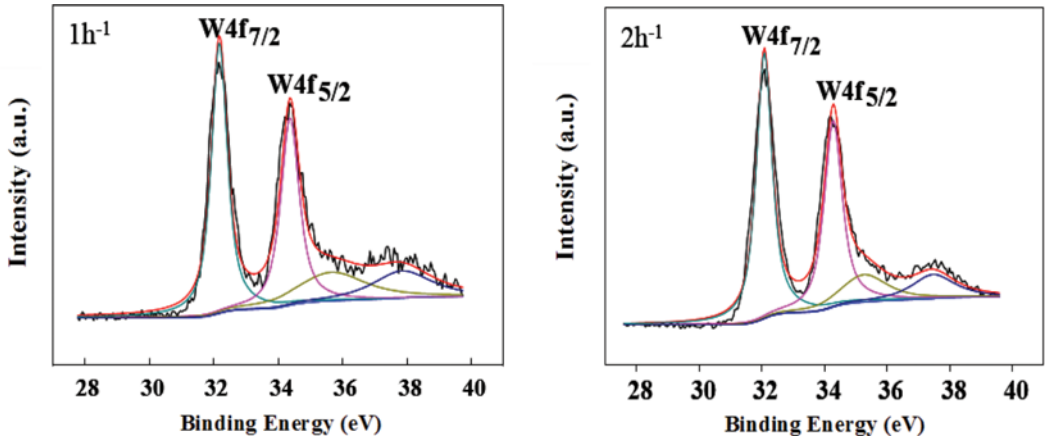

Fig. 8. W4f XPS spectra of the sulfided catalysts with different sulfiding LHSV.

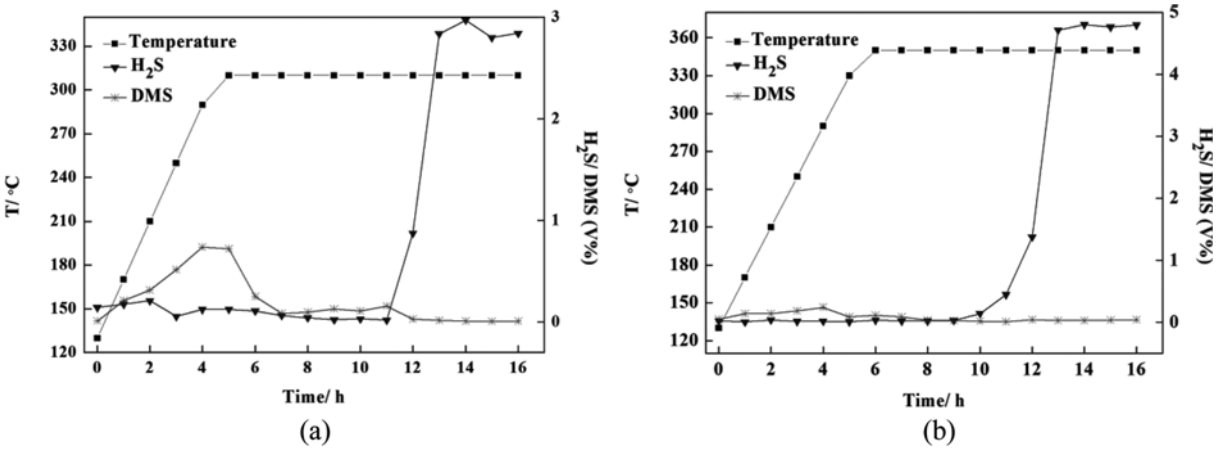

Fig. 9. Curves of temperature and content of main sulfides in exhaust changing with time with different sulfiding temperature ((a) 310 °C, (b) 350 °C).

centage of superficial fraction of both the W^{VI} and W^{IV} ions. From these data, it is deduced that the catalyst sulfided at 2 h^{-1} has a higher percentage of tungsten as WS_2 (76%) than the catalyst sulfided at 1 h^{-1} (68%).

2. Effect of Sulfiding Temperature

2-1. Sulfidation Process

The sulfidation of the catalyst precursor was carried out at three different temperatures (310, 330, and 350 °C) with a LHSV of 2 h^{-1} and a pressure of 6 MPa. The curves of the sulfiding temperature and the content of the sulfur compounds in the exhaust gas changing with the sulfiding time at different sulfiding temperature were obtained (310 °C: Fig. 9(a), 330 °C: Fig. 1(b), 350 °C: Fig. 9(b)). The reaction times of the sulfidation at 310, 330 and 350 °C were 8, 11, and 9 h, respectively. It showed that the necessary time needed for sulfidation at 330 °C was the longest.

2-2. Catalytic Activity

The X-ray diffraction patterns of the catalysts sulfided at different temperatures are shown in Fig. 10. The intensity of the MoS_2/WS_2 peaks was the highest when the sulfiding temperature was 330 °C, indicating that the MoS_2/WS_2 has higher degree of crystallinity at 330 °C. Therefore, the longest sulfiding time needed might be due to the sufficient sulfidation. Table 4 and Fig. 11 present the

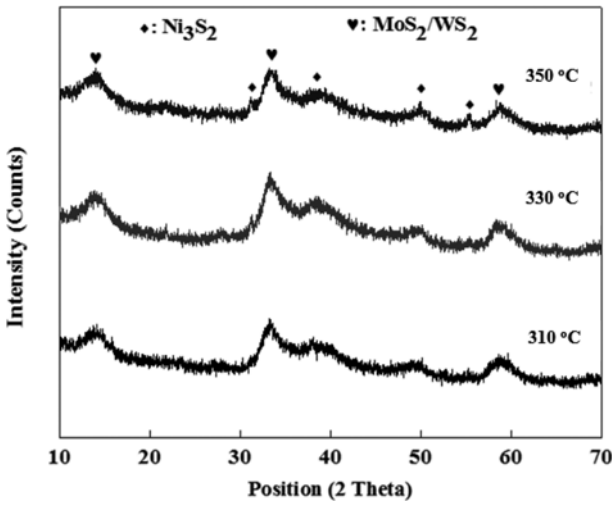

Fig. 10. XRD patterns of sulfided Ni-Mo-W catalysts with different sulfiding temperature.

activity data of the catalyst sulfided at different temperature. Table 4 shows that the gas oil density and the content of S and N in the

Table 4. Influence of sulfidation temperature on catalytic activities

Sulfiding temperature/°C	ρ/(g/mL)	S/(μg/g)	N/(μg/g)
Gas oil	0.8485	13940	161
310	0.8245	85.0	1.1
330	0.8243	63.4	0.8
350	0.8252	164.8	1.4

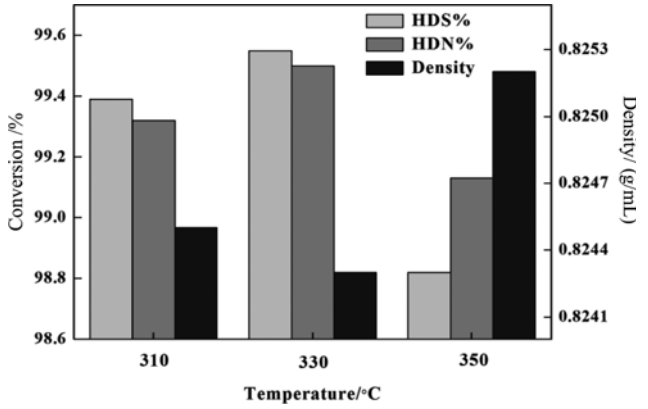

Fig. 11. Influence of sulfidation temperature on the activities of unsupported Ni-Mo-W catalysts.

gas oil decreased dramatically after catalytic hydrogenation. Fig. 11 shows that the catalyst sulfided at 330 °C had the highest activity, and both the desulfurization and denitrification degree of the catalyst reached over 99.5%, while the catalyst sulfided at 350 °C had the lowest activity.

Sulfiding at 330 °C was favorable for the formation of the MoS_2/WS_2 phase, which contributes to the higher activity of the catalyst with more active sites, while the diffraction peaks of Ni_3S_2 were more distinguishable in the catalyst sulfided at higher temperature. The sulfidation temperature of most NiMoW supported catalysts is higher than or equal to 400 °C [23,43], the reason might be due to the strong metal-support interaction in the supported catalyst resulted in the difficulty of reduction [44,45]. Our previous study

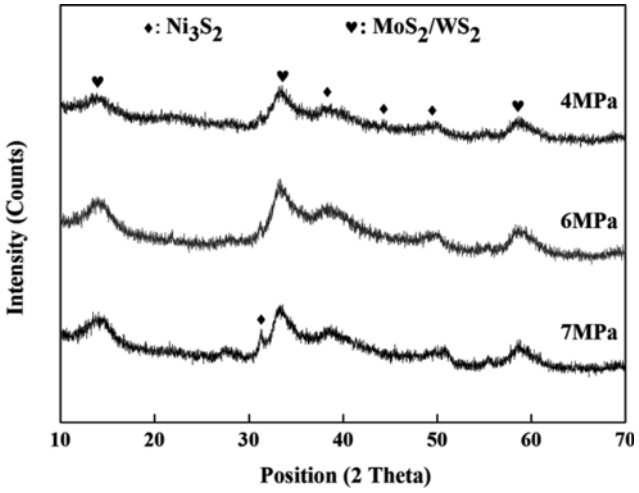

Fig. 13. XRD patterns of sulfided Ni-Mo-W catalysts with different sulfiding pressure.

showed that the higher sulfiding temperature, for unsupported catalyst, caused agglomeration of Ni_3S_2 species and an increase of the MoS_2/WS_2 slab length, which might be the reason for the low catalytic activity (Fig. 11) [46]. Therefore, 330 °C was the appropriate sulfiding temperature.

3. Effect of Sulfiding Pressure

3-1. Sulfidation Process

The sulfidation of the catalyst precursors was carried out at a pressure of 4 MPa (Fig. 12(a)), 6 MPa (Fig. 1(b)), and 7 MPa (Fig. 12(b)), with a LHSV of 2 h^{-1} and a temperature of 330 °C. The curves of the sulfiding temperature and the content of the main sulfur compounds in the exhaust gas changing with the time at different sulfiding pressure were obtained. The reaction times of the sulfidation at 4, 6, and 7 MPa were about 11, 11, and 10 h, respectively. Thus, the time needed for sulfidation of the catalysts sulfided at different pressure was almost the same.

3-2. Catalytic Activity

The X-ray diffraction patterns of the sulfided catalyst are shown in Fig. 13. The differences in the XRD patterns were not evident.

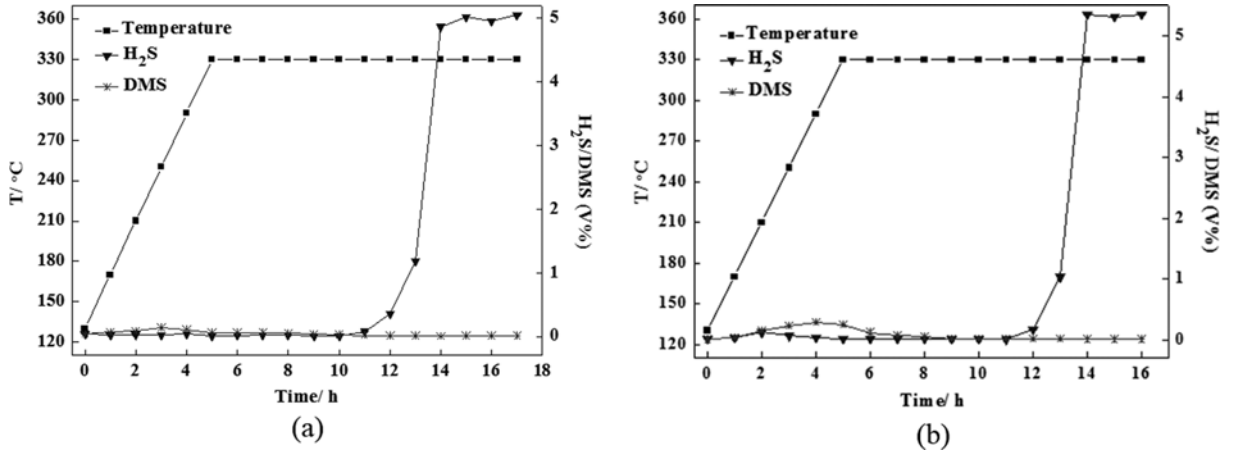

Fig. 12. Curves of temperature and content of main sulfides in exhaust changing with time with different sulfiding pressure ((a) 4 MPa, (b) 7 MPa).

Table 5. Influence of sulfidation pressure on catalytic activities

Sulfiding pressure/MPa	ρ/(g/mL)	S/(μg/g)	N/(μg/g)
Gas oil	0.8485	13940	161
4.0	0.8244	75.4	1.6
6.0	0.8243	63.4	0.8
7.0	0.8244	86.5	1.7

Table 5 presents the activity data of the catalyst sulfided at different pressure, and the result shows that the gas oil density and the content of S and N in the gas oil decreased dramatically after catalytic hydrogenation. The activities of the catalysts sulfided at different pressure were almost the same and both the desulfurization and denitrogenation degree of the catalysts reached over 99.5%. The results showed that the sulfidation pressure (within a given range) had little effect on the catalytic activity.

CONCLUSIONS

The effect of sulfiding conditions on the sulfidation behavior and activity of the unsupported Ni-Mo-W hydrotreating catalyst were investigated. The variation of the sulfur content in the exhaust showed that the reaction time necessary for the sulfidation decreased with increasing LHSV of sulfiding agent. However, the activity of the catalyst after sulfiding at 2 or 3 h^{-1} was higher than at 1 h^{-1}. The result might be attributed to the formation of the MoS_2/WS_2 slabs with shorter length and higher stacking number at relatively higher sulfiding LHSV, which could contribute to the higher hydrogenation ability. XPS results indicated that the fraction of nickel and tungsten sulfide phases of the catalyst sulfided at 2 h^{-1} was higher than the catalyst sulfided at 1 h^{-1}. This provides a useful reference for actual production, that an appropriate LHSV could not only improve the catalytic performance but also reduce the time needed for sulfidation without excessive consumption of sulfiding agent. Furthermore, the time needed for sulfidation was the longest when sulfiding at 330 °C, and the catalytic activity was also the highest after sulfiding at this temperature, which might be due to the fullest sulfidation with appropriate morphology of the catalyst. The sulfidation pressure had no significant effect on the catalytic behavior or activity in the range of test pressure. This characteristic provides great flexibility in determining ideal practical production conditions.

ACKNOWLEDGEMENTS

This work was financially supported by the National Key Fundamental Research Development Project of China (973 Project No. 2010CB226905) and the National Natural Science Fund of China (Grants nos. 21676301).

REFERENCES

1. A. Stanislaus, A. Marafi and M. S. Rana, *Catal. Today*, **153**, 1 (2010).
2. N. Wan, A. Wan and R. Ali, *React. Kinet. Mech. Catal.*, **114**, 547 (2014).
3. P. A. Nikulshin, D. I. Ishutenko, A. A. Mozhaev, K. I. Maslakov and A. A. Pimerzin, *J. Catal.*, **312**, 152 (2014).
4. Y. Gochi, C. Ornelas, F. Paraguay, S. Fuentes, L. Alvarez, J. L. Rico and G. Alonso-Núñez, *Catal. Today*, **107**, 531 (2005).
5. F. L. Plantenga, R. Cerfontain, S. Eijsbouts, F. V. Houtert, G. H. Anderson, S. Miseo, S. Soled, K. Riley, K. Fujita and Y. Inoue, *Stud. Surf. Sci. Catal.*, **145**, 407 (2003).
6. S. Eijsbouts, S. W. Mayo and K. Fujita, *Appl. Catal. A: Gen.*, **322**, 58 (2007).
7. H. Liu, C. Liu, C. Yin, Y. Chai, Y. Li, D. Liu, B. Liu, X. Li, Y. Wang and X. Li, *Appl. Catal. B: Environ.*, **174**, 264 (2015).
8. C. Liu, H. Liu, C. Yin, X. Zhao, B. Liu, X. Li, Y. Li and Y. Liu, *Fuel*, **154**, 88 (2015).
9. Y. Duan, S. Zhang and K. Hou, *J. Chem. Eng. Chin. Univ.*, **26**, 449 (2012).
10. C. Yin, L. Zhao, Z. Bai, H. Liu, Y. Liu and C. Liu, *Fuel*, **107**, 873 (2013).
11. T. Kubota, N. Miyamoto, M. Yoshioka and Y. Okamoto, *Appl. Catal. A: Gen.*, **480**, 10 (2014).
12. J. A. Lumbreras, R. Huirache-Acuña, E. M. Rivera-Muñoz, G. Berhault and G. Alonso-Núñez, *Catal. Lett.*, **134**, 138 (2010).
13. G. Berhault, L. C. Araiza, A. D. Moller, A. Mehta and R. R. Chianelli, *Catal. Lett.*, **78**, 81 (2002).
14. G. Marroquín, J. Ancheyta and J. A. I. Díaz, *Catal. Today*, **98**, 75 (2004).
15. Z. Li, J. Liu, H. Wang, E. Wang, B. Wang, X. Ma, S. Qin and Q. Sun, *J. Mol. Catal. A: Chem.*, **378**, 99 (2013).
16. H. G. Füchtbauer, A. K. Tuxen, Z. Li, H. Topsøe, J. V. Lauritsen and F. Besenbacher, *Top. Catal.*, **57**, 207 (2014).
17. P. G. Moses, B. Hinneman, H. Topsøe and J. K. Nørskov, *J. Catal.*, **2**, 188 (2007).
18. L. P. Hansen, Q. M. Ramass, K. Christian, B. Michael, J. Erik, T. Henrik and H. Stig, *Angew. Chem.*, **50**, 10153 (2011).
19. G. Berhault, A. Mehta, A. C. Pavel, J. Yang, L. Rendon, M. J. Yácaman, L. C. Araiza, A. D. Moller and R. R. Chianelli, *J. Catal.*, **198**, 9 (2001).
20. L. Oliviero, L. Mariey, M. A. Lélias, S. Aiello, J. V. Gestel and F. Maugé, *Catal. Lett.*, **135**, 62 (2010).
21. Y. Okamoto, K. Hioka, K. Arakawa, T. Fujikawa, T. Ebihara and T. Kubota, *J. Catal.*, **268**, 49 (2009).
22. J. S. Chan, K. Chan and H. M. Sang, *Catal. Today*, **74**, 193 (2002).
23. S. L. Amaya, G. Alonso-Núñez, T. A. Zepeda, S. Fuentes and A. Echavarría, *Appl. Catal. B: Environ.*, **148**, 221 (2014).
24. S. L. Amaya, G. Alonso-Núñez, J. Cruz-Reyes, S. Fuentes and A. Echavarría, *Fuel*, **139**, 575 (2015).
25. A. I. Dugulan, E. J. M. Hensen and J. A. R. V. Veen, *Catal. Today*, **130**, 126 (2008).
26. H. Topsøe and B. S. Clausen, *Catal. Rev.*, **26**, 395 (1984).
27. T. Samuel, B. Gilles, P. Guy, H. Virginie and D. Fabrice, *J. Catal.*, **223**, 404 (2004).
28. R. Huirache-Acuña, M. A. Albiter, J. Espino, C. Ornelas, G. Alonso-Nuñez, F. Paraguay-Delgado, J. L. Rico and R. Martínez-Sánchez, *Appl. Catal. A: Gen.*, **304**, 124 (2006).
29. R. Huirache-Acuña, M. A. Albiter, C. Ornelas, F. Paraguay-Delgado, R. Martínez-Sánchez and G. Alonso-Nuñez, *Appl. Catal. A: Gen.*, **308**, 134 (2006).
30. L. Liu, D. Liu, B. Liu, G. Liu, Y. Liu and C. Liu, *J. Fuel Chem. Tech-*

nol., **39**, 838 (2011).
31. L. Vradman, M. V. Landau and M. Herskowitz, *Fuel*, **82**, 633 (2003).
32. E. Altamirano, J. A. D. L. Reyes, F. Murrieta and M. Vrinat, *J. Catal*., **235**, 403 (2005).
33. B. Yoosuk, C. Song, J. H. Kim, C. Ngamcharussrivichai and P. Prasassarakich, *Catal. Today*, **149**, 52 (2010).
34. L. S. Byskov, B. Hammer, J. K. Nørskov, B. S. Clausen and H. Topsøe, *Catal. Lett*., **47**, 177 (1997).
35. L. Peña, D. Valencia and T. Klimova, *Appl. Catal. B: Environ*., **147**, 879 (2014).
36. W. Lai, W. Song, L. Pang, Z. Wu, N. Zheng, J. Li, J. Zheng, X. Yi and W. Fang, *J. Catal*., **303**, 80 (2013).
37. E. Rodríguez-Castellón, A. Jiménez-López and D. Eliche-Quesada, *Fuel*, **87**, 1195 (2008).
38. J. Juan-Juan, M. C. Román-Martínez and M. J. Illán-Gómez, *Appl. Catal. A: Gen*., **355**, 27 (2009).
39. L. Benoist, D. Gonbeau, G. Pfister-Guillouzo, E. Schmidt, G. Meunier and A. Levasseur, *Thin Solid Films*, **258**, 110 (1995).
40. D. Zuo, M. Vrinat, H. Nie, F. Maugé, Y. Shi, M. Lacroix and D. Li, *Catal. Today*, **93**, 751 (2004).
41. L. J. Salvati, L. E. Makovsky, J. M. Stencel, F. R. Brown and D. M. Hercules, *ChemInform*, **84:22**, 2898 (1982).
42. J. RamíRez and A. Gutiérrez-Alejandre, *Catal. Today*, **43**, 123 (1998).
43. J. A. Mendoza-Nieto, O. Vera-Vallejo, L. Escobar-Alarcón, D. Solís-Casados and T. Klimova, *Fuel*, **110**, 268 (2013).
44. P. Jabbarnezhad, M. Haghighi and P. Taghavinezhad, *Korean J. Chem. Eng*., **32**, 1258 (2015).
45. H. M. Koo, G. Y. Han and J. W. Bae, *Korean J. Chem. Eng*., **33**, 1565 (2016).
46. C. Yin, Y. Wang, S. Xue, H. Liu, H. Li and C. Liu, *Fuel*, **175**, 13 (2016).